Published in final edited form as:
Nat Cell Biol. 2011 May ; 13(5): 599–610. doi:10.1038/ncb2213.

Meiotic homologous chromosome alignment and its surveillance are controlled by mouse HORMAD1

Katrin Daniel[1], **Julian Lange**[2], **Khaled Hached**[3,4], **Jun Fu**[5], **Konstantinos Anastassiadis**[6], **Ignasi Roig**[2,7], **Howard J. Cooke**[8], **A. Francis Stewart**[5], **Katja Wassmann**[3,4], **Maria Jasin**[9], **Scott Keeney**[2,10], and **Attila Tóth**[1]

[1] Institute of Physiological Chemistry, Technische Universität Dresden, Fiedlerstrasse 42, 01307 Dresden, Germany

[2] Molecular Biology Program, Memorial Sloan-Kettering Cancer Center, New York, NY 10065, USA

[3] CNRS UMR7622 Biologie du Développement Paris 6, 9 quai St. Bernard, Paris, 75005 France

[4] UPMC Paris 6, 9 quai St. Bernard, Paris, 75005 France

[5]Genomics, BioInnovationsZentrum, Technische Universität Dresden, Am Tatzberg 47, 01307 Dresden, Germany

[6] Center for Regenerative Therapies Dresden, BioInnovationsZentrum, Technische Universität Dresden, Am Tatzberg 47, 01307 Dresden, Germany

[8]MRC Human Genetics Unit, Western General Hospital, Crewe Road, Edinburgh, EH4 2XU, UK

[9] Developmental Biology Program, Memorial Sloan-Kettering Cancer Center, New York, NY 10065, USA

[10] Howard Hughes Medical Institute, Memorial Sloan-Kettering Cancer Center, New York, NY 10065, USA

Abstract

Meiotic crossover (CO) formation between homologous chromosomes (homologues) entails DNA double strand break (DSB) formation, homology search using DSB ends, and synaptonemal complex (SC) formation coupled with DSB repair. Meiotic progression must be prevented until DSB repair and homologue alignment are completed to avoid forming aneuploid gametes. Here we show that mouse HORMAD1 ensures that sufficient numbers of processed DSBs are available for successful homology search. HORMAD1 is needed for normal SC formation and for the efficient recruitment of ATR checkpoint kinase activity to unsynapsed chromatin. The latter phenomenon was proposed to be important in meiotic prophase checkpoints in both sexes. Consistent with this hypothesis, HORMAD1 is essential for the elimination of SC-defective

Correspondence should be addressed to AT.
[7]Present address: Unitat de Citologia i Histologia, Dept. Biologia Cel·lular, Fisiologia i Immunologia, Facultat de Biociències, Universitat Autònoma de Barcelona, Cerdanyola del Vallès, 08193, Spain

AUTHOR CONTRIBUTIONS

K.D. designed, performed and analysed most of the experiments; J.L., I.R., M.J. and S.K. contributed with SPO11-oligo measurements; J.F., K.A. and A.F.S. designed and generated the targeting construct and targeted ES cells; K.H. and K.W. carried out oocyte maturation experiments and oocyte video microscopy; H.J.K. provided the *Syce2+/−* mouse, A.T. was involved in oocyte maturation experiments and oocyte counts, helped K.D. in experimental design and wrote the paper together with K.D. All authors were involved in discussions and commented on the manuscript.

COMPETING FINANCIAL INTERESTS

The authors declare no competing financial interest

oocytes. SC formation results in HORMAD1 depletion from chromosome axes. Thus, we propose that SC and HORMAD1 are key components of a negative feedback loop that coordinates meiotic progression with homologue alignment: HORMAD1 promotes homologue alignment and SC formation, and SCs down-regulate HORMAD1 function, thereby permitting progression past meiotic prophase checkpoints.

INTRODUCTION

Physical linkages between homologues ensure correct chromosome segregation during the first meiotic division in mammals. These physical linkages, called chiasmata, depend on the formation of at least one reciprocal recombination event, or CO, between each homologue pair and on cohesion between pairs of sister chromatids (Supplementary Information, Fig. S1a)[1, 2]. CO formation begins with the introduction of DSBs into the genome by the SPO11 enzyme (Supplementary Information, Fig. S1)[3-5]. DSBs are processed to produce single-stranded DNA ends that can be used to probe for homology through strand invasion[6]. Several DSB ends work together on each homologue pair to ensure successful homologue alignment. After successful homology search, SCs form and connect the axes of aligned homologues. SC components promote post-homology search steps in DSB repair and are required for efficient CO formation[1, 2]. After SCs formation, homology search is no longer needed, most DSBs become repaired from homologues as non-crossovers, and at least one DSB per chromosome pair is turned into a CO[1, 2]. In mammals, meiotic checkpoint mechanisms eliminate meiocytes with defects in homologue alignment and DSB repair during the first meiotic prophase, thereby ensuring that it is rare for gametes to form with an abnormal chromosome set or with unrepaired DNA[7-14]. Despite the importance of these meiotic prophase checkpoint mechanisms, they are poorly understood.

In various non-mammalian taxa, meiotic HORMA (Hop1, Rev7 and Mad2)-domain proteins have been implicated in diverse processes linked to CO formation[2, 15-38]. These include DSB formation, homology search, preferred use of homologous DNA over sister DNA for repair of DSBs, SC formation and the meiotic prophase checkpoint. Here we address the functions of HORMAD1, one of two meiosis-specific mouse HORMA-domain proteins (HORMAD1 and HORMAD2) that were shown to preferentially associate with unsynapsed chromosome axes during first meiotic prophase in mice[39-41].

RESULTS

HORMAD1 is required for fertility

Reasoning that functional analysis of HORMADs might provide novel insights into meiotic chromosome behaviour and CO formation in mammals, we disrupted *Hormad1* in mouse (Supplementary Information, Fig. S2). While no obvious somatic defects were observed in *Hormad1*$^{-/-}$ mice, both sexes are sterile, as reported by others as well[41]. Although spermatocytes in *Hormad1*$^{-/-}$ mice are present in testis tubules at epithelial cycle stage III-IV, which we identified by the presence of intermediate spermatogonia[42], they undergo apoptosis by the end of stage IV, and post-meiotic cells are not found in *Hormad1*$^{-/-}$ testes (Supplementary Information, Fig. S3). In wild type (WT), stage IV tubules contain mid-pachytene spermatocytes[42]; thus *Hormad1*$^{-/-}$ spermatocytes are eliminated at a stage equivalent to mid-pachytene. Since spermatocytes with defects in SC formation and DSB repair are eliminated by the mid-pachytene checkpoint[7-14] we examined SC formation on nuclear surface spreads of *Hormad1*$^{-/-}$ spermatocytes.

HORMAD1 promotes SC formation

In WT spermatocytes, chromosome axes are fully formed by late-zygotene and SC formation on autosomes is completed by pachytene (Fig. 1a, b). While chromosome axis-cohesion core development and the timing of SC formation are similar in WT and *Hormad1 −/−* spermatocytes, the efficiency of stable SC initiation and SC elongation is reduced in the mutant (Fig. 1c, Supplementary Information, Fig. S4). Autosomal SC formation is never completed in *Hormad1 −/−* cells with fully formed chromosome axes (n=1000); most chromosomes that start SC formation do not complete it, and many chromosomes do not even partially synapse (Fig. 1c). Due to these defects we cannot distinguish between late-zygotene and pachytene in mutant spermatocytes and we refer to these stages as zygotene-pachytene. Unlike in SC transverse filament mutant meiocytes, where unsynapsed chromosomes align along their length[8-11], unsynapsed chromosomes do not align in *Hormad1 −/−* spermatocytes (Fig. 1c). Nevertheless, based on the similar axis lengths of synapsed chromosomes, the relatively long stretches of SCs that frequently form in zygotene-pachytene *Hormad1 −/−* spermatocytes appear to connect homologues (Fig. 1c). SC formation between non-homologous chromosomes is unambiguously identifiable only in a small fraction of *Hormad1 −/−* spermatocytes (2.3% n=174) (data not shown). Similar homologue alignment and SC formation defects are found in *Hormad1 −/−* oocytes (Supplementary Information, Fig. S5). Others reported complete lack of SCs in *Hormad1 −/−* spermatocytes based on the lack of tripartite SC structures observable by electron microscopy[41]. The different conclusion reached by us may reflect differences in strain backgrounds and/or SC detection methods in the two studies.

Homologue alignment defects could explain the SC defects in the *Hormad1 −/−* mutant. Additionally, HORMAD1 may also have SC promoting functions independent of its role in homologue alignment. To test this possibility, we examined the effect of the *Hormad1* mutation in the DSB-deficient *Spo11 −/−* background, where homology search fails and SCs form extensively between non-homologous partners (Fig. 1)[4, 5]. If HORMAD1 promotes SC formation only through a function in DSB repair and homologue alignment, *Spo11 −/− Hormad1 −/−* double mutant meiocytes should be as proficient in non-homologous SC formation as *Spo11 −/−* single mutant meiocytes. Notably, the double mutant has a much more severe SC defect than either single mutant in both sexes (Fig. 1, Supplementary Information, Fig. S5). It is unlikely that the double mutant SC-phenotype is caused by an early block in meiotic progression, because single and double mutant spermatocytes are eliminated at a comparable stage (Supplementary Information, Fig. S6). Hence, our findings indicate that HORMAD1 promotes SC formation independent of homology search and raise the possibility that HORMAD1 has a direct role in SC formation.

HORMAD1, DSB formation and DSB repair

Early DSB repair steps are important for homology search. Therefore, we examined if chromosome alignment-SC defects in *Hormad1 −/−* meiocytes reflect DSB repair defects. The first step in DSB repair is DNA end resection, which creates single-stranded 3′ overhangs bound by two recombinases, RAD51 and DMC1, that facilitate homology search[1, 2, 6, 43-45]. RAD51- and DMC1-marked meiotic DSB sites are chromosome axes-associated, and RAD51-DMC1 focus counts provide an estimate of the number of DSBs available for homology search[1]. Upon SC formation, RAD51 and DMC1 are replaced at most DSB sites by markers of intermediate stages of DSB repair, including the single-stranded DNA binding protein RPA and MSH4[1, 46]. RAD51, DMC1, RPA and MSH4 foci numbers are significantly lower in *Hormad1 −/−* spermatocytes than in WT cells during observable prophase stages (Fig. 2a-h, Supplementary Information, Fig. S7a-d)[41]. During the comparable early-mid-zygotene stage median foci numbers are three- to six-fold reduced in *Hormad1 −/−* spermatocytes. (Fig. 2e-h). RAD51 and RPA focus numbers are similarly

reduced in *Hormad1*−/− oocytes (Supplementary Information, Fig. S7e, f)[41]. Thus the steady state numbers of single-stranded DSB ends appear strongly reduced in *Hormad1*−/− meiocytes, which could explain the inefficient homologue alignment and contribute to defective SC formation.

Two scenarios could explain the reduced numbers of processed DSB ends in *Hormad1*−/− meiocytes: either fewer processed DSBs are produced, or DSBs are repaired faster. Recombination protein foci first appeared at similar times (but fewer in number) and did not disappear prematurely in *Hormad1*−/− spermatocytes (Fig. 2e-h). In particular, we did not see dramatic early decline in RPA focus numbers, which would indicate premature repair. We also examined the behaviour of the late recombination marker MLH1, which appears at destined CO sites from mid-pachytene onwards in WT (Fig. 2i-k)[46-48]. We never observed MLH1 foci in *Hormad1*−/− spermatocytes (n=378). Defective MLH1 foci formation in *Hormad1*−/− spermatocytes[41] is unlikely to be the result of a direct block in DSB repair, because MLH1 foci are detected (preferentially associated with synapsed axes) in *Hormad1*−/− oocytes, albeit in reduced numbers (~30% of WT) (Fig. 2i-k). This difference between oocytes and spermatocytes is likely due to different timing of elimination of defective meiocytes, with oocytes eliminated later, allowing stages corresponding to late-pachytene to be examined. Although we cannot exclude that some DSB repair steps are accelerated in *Hormad1*−/− meiocytes, the behaviour of recombination proteins does not indicate significant acceleration.

We next asked how efficiently DSBs and/or single-stranded DSB ends are produced in the *Hormad1*−/− mutant. DSBs trigger accumulation of phospho-histone H2AX (γH2AX) during leptotene-early-zygotene through activation of ATM kinase[49, 50]. Levels of chromatin-bound γH2AX are significantly reduced in *Hormad1*−/− leptotene-early-zygotene spermatocytes (Supplementary Information, Fig. S8). Consistent with this, others reported reduced γH2AX levels and reduced ATM autophosphorylation, implying reduced ATM activation, in *Hormad1*−/− spermatocytes[41].

Since this result may indicate reduced DSB formation, we measured the effect of *Hormad1*−/− mutation on amounts of SPO11-oligonucleotide complexes that are produced when DSB ends are resected[45] (Fig. 3a-d). To control for the fact that the *Hormad1*−/− mutant displays a mid-pachytene spermatogenic block, we employed the DSB repair-defective *Dmc1*−/− background: DMC1-deficient spermatocytes arrest in mid-pachytene irrespective of *Hormad1* genotype (Fig. 3e)[12, 43, 44]. In three independent experiments with adult mice we observed 2-, 3.1- and 4.2-fold reduction in testis-weight-normalised SPO11-oligonucleotide levels in *Hormad1*−/− *Dmc1*−/− testes relative to *Hormad1*+/+ *Dmc1*−/− controls (Fig. 3a). We also examined SPO11-oligonucleotide levels in testes of juvenile 14 days postpartum-dpp mice (Fig. 3c), in which the sizes and cellularities of WT and mutant testes are comparable because the vast majority of spermatocytes have not yet progressed far enough in meiosis to be affected by the mid-pachytene checkpoint. In two independent experiments testis-weight-normalised SPO11-oligonucleotide levels were reduced 3.8- and 4.8-fold in *Hormad1*−/− testes relative to WT controls, whereas WT and *Dmc1*−/− testes were similar. Although we cannot exclude that turnover of both SPO11-oligonucleotide complexes and single-stranded DSB ends are faster in the *Hormad1*−/− mutant, the simplest interpretation of our observations is that HORMAD1 is needed for efficient formation of DSBs and/or single-stranded DSB ends.

HORMAD1 and meiotic prophase checkpoints

Collaboration between Hop1 and Mec1, the yeast orthologues of HORMAD1 and ATR respectively, is required for the meiotic prophase checkpoint in budding yeast[35]. Interestingly, HORMAD1 preferentially associates with unsynapsed chromosome axes,

resembling the behaviour of ATR and two ATR activators, BRCA1 and TOPBP1 in WT meiocytes[51-57]. Active ATR phosphorylates H2AX on unsynapsed chromatin from zygotene onwards, thereby promoting meiotic silencing of unsynapsed chromosomes (MSUC), a phenomenon that is crucial for the mid-pachytene checkpoint[13, 14, 57]. Therefore, we asked whether HORMAD1 also has a role in these processes. In spermatocytes, sex chromosomes only synapse and recombine in their short pseudoautosomal regions. Consequently, most sex chromosome regions remain unsynapsed and silenced in a γH2AX-rich structure termed the sex body[57-59]. Efficient sex chromosome silencing is essential for progression beyond mid-pachytene[60, 61]. In DSB repair-SC defective spermatocytes, ATR activity (γH2AX) persists on unsynapsed autosomes, and fails to accumulate strongly on sex chromosomes[8-12, 60]. Consequently, sex body formation and sex chromosome silencing fail, resulting in mid-pachytene apoptosis[60, 61]. Sex body formation is defective in *Hormad1*−/− spermatocytes (Fig. 4a)[41]. Nevertheless, γH2AX was observed accumulating in chromatin regions that are not associated strongly with unsynapsed chromosome axes in *Hormad1*−/− spermatocytes. This abnormal localisation of γH2AX could result either from reduced DSB numbers and incomplete SC formation or from a more direct involvement of HORMAD1 in the recruitment of ATR activity to unsynapsed chromatin.

To test these two possibilities, we examined the effect of *Hormad1*−/− mutation on the MSUC pathway in a *Spo11*−/− background[4, 5]. Although SC formation is abnormal in *Spo11*−/− spermatocytes, MSUC is active and a random subset of unsynapsed chromosome axes is frequently associated with one or a few γH2AX-rich silenced chromatin domains termed pseudo-sex bodies (Fig. 4b)[12, 50]. Since SC formation is severely compromised in *Hormad1*−/− *Spo11*−/− meiocytes relative to *Spo11*−/− mutants (Fig. 1), we controlled for loss of SCs by comparing pseudo-sex body formation and the behaviour of MSUC proteins in the *Hormad1*−/− *Spo11*−/− double mutant with the *Syce2*−/− *Spo11*−/− double mutant, which lacks an SC central element component and does not form SCs[9]. Formation of pseudo-sex body-like chromatin domains is strongly reduced in *Hormad1*−/− *Spo11*−/− double mutant spermatocytes relative to both *Spo11*−/− and *Syce2*−/− *Spo11*−/− controls (Fig. 4b, c). Lack of HORMAD1 strongly reduces total nuclear γH2AX immunofluorescence staining in the *Spo11*−/− background, whereas loss of SC formation does not (Fig. 4d). Both ATR and TOPBP1 accumulate within pseudo-sex bodies, and BRCA1 accumulates on chromosome axes associated with pseudo-sex bodies (Fig. 5)[12, 50, 60]. We observed reduced localisation of TOPBP1, ATR and BRCA1 to unsynapsed chromatin in the *Hormad1*−/− *Spo11*−/− double mutant in comparison with both control strains (Fig. 5). This phenotype is probably not caused by an early block in meiotic progression, since *Spo11*−/−, *Syce2*−/− *Spo11*−/− and *Hormad1*−/− *Spo11*−/− spermatocytes are eliminated in stage IV tubules (Supplementary Information, Fig. S6). The most straightforward interpretation is that HORMAD1 promotes recruitment of MSUC proteins to unsynapsed chromatin regions independently of its role in the formation of processed DSBs and SCs.

The prophase checkpoint is less well understood in oocytes than in spermatocytes, although ATR activation and MSUC has been implicated in the female checkpoint[13, 57]. In the absence of heterologous sex chromosomes, oocytes do not form sex bodies. Nevertheless *Spo11*−/− oocytes frequently contain male pseudo-sex body-like γH2AX-rich chromatin domains that also contain TOPBP1 and BRCA1 (Supplementary Information, Fig. S9)[13]. Formation of such female “pseudo-sex bodies” is strongly reduced in *Hormad1*−/− *Spo11*−/− oocytes (Supplementary Information, Fig. S9), indicating that HORMAD1 may have a role in MSUC and the prophase checkpoint in females. Therefore, we compared the number of oocytes in ovaries from 6-weeks-old WT, *Hormad1*−/−, *Spo11*−/− and *Hormad1*−/− *Spo11*−/− animals and in ovaries from 11-month-old WT and *Hormad1*−/− animals (Fig. 6a, b). In the SC-defective *Spo11*−/− mutant, very few oocytes survive until 6 weeks.

Despite defective SC formation, oocyte numbers are not reduced in *Hormad1−/−*[41] or *Hormad1−/− Spo11−/−* animals relative to WT. Notably, oocyte apoptosis rates are similar in WT, *Hormad1−/−* and *Hormad1−/− Spo11−/−* mice, and are greatly elevated in the *Spo11−/−* mutant one day after birth, when many of the SC-defective oocytes are eliminated (Fig. 6c). Thus, *Hormad1−/−* suppresses oocyte loss in the *Spo11−/−* background. These observations demonstrate that HORMAD1 is essential for the female prophase checkpoint that eliminates oocytes with abnormal SC formation and homologue alignment.

Chromosome segregation in *Hormad1−/−* oocytes

Follicular oocyte development does not require HORMAD1[41] since we found oocytes at all stages of follicular development in *Hormad1−/−* and *Hormad1−/− Spo11−/−* animals (Fig. 6a). This allowed us to test whether chiasmata form during the first meiotic metaphase in the absence of HORMAD1. On average, roughly one third of chromosomes were connected by chiasmata in *in vitro*-matured metaphase *Hormad1−/−* oocytes, which corresponds well to the number of MLH1 foci observed in pachytene oocytes (Fig. 2k, 7). Chiasmata formation depends both on sister chromatid cohesion along chromosome arms and on CO formation. Thus, our observations suggest that sister chromatid cohesion is intact and that MLH1-marked DSB sites are efficiently resolved as COs in the *Hormad1−/−* mutant.

We evaluated the consequences of reduced CO numbers on the first meiotic division in *in vitro*-matured oocytes. Although nuclear envelope breakdown efficiency was similar in WT (142 of 149) and *Hormad1−/−* (73 of 77) oocytes, polar body extrusion was greatly reduced in the mutant (5 of 60) relative to WT (92 of 95). Video microscopy shows that *Hormad1−/−* oocytes have abnormally long meiosis I spindles, on which chromosomes fail to align (Fig. 7c, d, Supplementary Information, Movies 1, 2). This defect likely causes anaphase failure and the polar body extrusion defect. Despite the abnormal first meiotic division, some of the *Hormad1−/−* oocytes are fertilised *in vivo* since in a few cases (3 of 11 breeding pairs) we found one to three reabsorbing embryos five to eight days after breeding began. Nevertheless, embryos never developed to full term in *Hormad1−/−* females (19 females, 125 breeding weeks). Infertility and loss of embryos are consistent with the meiotic chromosome segregation defects (Fig. 7c, d, Supplementary Information, Movies 1, 2) and with the reported widespread aneuloidy in early embryos in *Hormad1−/−* females[41].

DISCUSSION

We analysed the functions of HORMAD1 using mouse genetics. We propose three distinct biological functions for mouse HORMAD1. First, HORMAD1 increases the steady state numbers of single-stranded DSB ends, thereby facilitating homology search. Our data suggest that HORMAD1 promotes either efficient DSB formation or resection of DSB ends or both. Because budding yeast Hop1 is required for efficient DSB formation[29, 35] we favour the first possibility. In budding yeast, inter-homologue CO numbers remain relatively stable when DSB numbers are reduced, a phenomenon called CO homeostasis[62]. Comparable reduction in the numbers of early-intermediate recombination protein foci (particularly RPA) and of chiasmata in the *Hormad1−/−* mutant might be interpreted as a sign of lack of CO homeostasis in mice (Fig. 2, [7]). However, a trivial explanation is that CO homeostasis can function only if homology search succeeds and homologues align. Hence, the roughly three-fold reduction in CO formation may simply reflect the low number of homologues that manage to partially or fully align in *Hormad1−/−* meiocytes. The observed correlation between numbers of SYCP1 stretches and MLH1 foci in oocytes is consistent with this latter possibility (Fig. 2j). Our data suggest that *Hormad1−/−* meiocytes are proficient in DSB repair steps that are important for homology search and inter-homologue CO formation, and reduced CO formation is caused by reduced levels of single-stranded DSB ends. Consistently with this hypothesis some homologues appear to synapse at least

partially in *Hormad1 −/−* meiocytes, a conclusion based on the observations that incomplete SCs form between chomosomes of similar axis length, and that SC formation largely depends on SPO11-DSBs and presumably on the downstream process of homology search in *Hormad1 −/−* cells (Fig. 1, Supplementary Information, Fig. S5). Furthermore, chiasmata form between chromosomes of identical length indicating that inter-homologue chiasmata, which are consequences of inter-homologue COs, form in *Hormad1 −/−* oocytes (Fig. 7a).

Second, HORMAD1 promotes SC formation independently of its role in homology search. This conclusion is based on the observation that HORMAD1 is needed for efficient non-homologous SC formation (Fig. 1, Supplementary Information, Fig. S5). It is formally possible that HORMAD1 is required only for pathological non-homologous synapsis. However, we consider it unlikely that as a prelude to homology search unsynapsed chromosome axes are loaded with a protein (HORMAD1) that specifically promotes non-homologous synapsis. It seems more likely that HORMAD1 promotes SC formation between axes that come into close proximity, irrespective of underlying homology.

Finally, HORMAD1 plays a key role in the male mid-pachytene checkpoint and the female meiotic prophase checkpoint, both of which eliminate meiocytes with defects in DSB repair and/or in homologue alignment-SC formation. HORMAD1 is required for efficient build up of ATR activity on unsynapsed chromosome regions, a process that is believed to form the basis of MSUC and meiotic prophase quality control in both sexes[13, 14, 57] (Fig. 4, 5, Supplementary Information, Fig. S9). In males, mid-pachytene apoptosis of DSB repair-SC defective spermatocytes is triggered by failure of MSUC on sex chromosomes, allowing transcription of genes whose expression is incompatible with survival beyond mid-pachytene[13, 60, 61]. In females, elimination of defective oocytes might be triggered by inappropriate MSUC or persistent ATR activity during prophase[13]. Therefore, the apparently opposite effect of *Hormad1* mutation in the two sexes (i.e., apoptosis of spermatocytes and survival of SC-defective oocytes) is likely caused by a common defect in recruitment of ATR activity to unsynapsed chromosomes. ATR is recruited to DSB sites in somatic cells, where it becomes active as part of the G2/M DSB repair checkpoint[14]. In meiosis, ATR and its activators are recruited to both DSB sites and unsynapsed chromatin[13, 14, 51-57, 60]. Our data raise the possibility that HORMAD1 fulfils its role in meiotic progression control by recruiting ATR and/or other components of the somatic DSB checkpoint machinery to unsynapsed chromatin, thereby adapting their functions for the detection of unsynapsed chromosome axes.

A comprehensive model for meiotic progression control emerges from this study and previous work showing that HORMAD1 is depleted from chromosome axes in response to SC formation (Fig. 8)[40]. We propose that the SC and HORMAD1 interact in a negative feedback-loop, to coordinate meiotic progression with successful homologue alignment. HORMAD1 promotes homologue alignment and SC formation. In turn, SC formation down-regulates HORMAD1 function by promoting HORMAD1 depletion from aligned homologues, which is a prerequisite for progression beyond the first meiotic prophase.

Although our observations and consistent observations of others[41] clearly show the importance of HORMAD1 during mice meiosis, *Hormad1 −/−* phenotypes appear partial. Conceivably, HORMAD1's paralogue, HORMAD2, might partially substitute for HORMAD1 during meiosis. It will be possible to resolve this question through analysis of *Hormad1 −/− Hormad2 −/−* mice when such mutant becomes available.

Methods

Hormad1 targeting

The *Hormad1* targeting construct was designed according to the multi-purpose allele strategy[63]. The Splice-Acceptor (SA)-IRES-LacZneo-pA and PGK-Blasticidin-pA cassettes flanked by FRT sites were inserted in intron 3 (Supplementary Information, Fig. S2). The frame-shifting exon 4 was flanked by loxP sites. Plasmids were constructed using recombineering methods available on request[64]. To modify the *Hormad1* locus, mouse R1 embryonic stem (ES) cells were cultured (using Mitomycin-C inactivated mouse embryonic fibroblasts as feeders) and electroporated with the linearised targeting constructs using standard protocols. Southern blot was used to identify correctly targeted ES clones: DNA was digested overnight with BclI, Bsu36I or HindIII for Southern blots with internal-, 5′- or 3′-probe, respectively, and DNA fragments were separated on 0.8% agarose gels (data not shown).

Generation of knockouts and genotyping

We generated mice that carried either of two different *Hormad1* null alleles (*Hormad1*^{insertion} and *Hormad1*^{deletion}) or an allele with restored functionality (*Hormad1*^{restored}) (Supplementary Information, Fig. S2). Two independent ES cell clones with a single integration of the targeting construct into the *Hormad1* locus were used to generate chimeric animals. Progeny of the chimeric animals crossed to C57BL/6JOlaHsd females were genotyped by Southern blot and PCR (Supplementary Information, Fig. S2). In subsequent crosses, only PCR was used for genotyping the various alleles of *Hormad1* from tail tip DNA. Genotyping primers: LacZfor 5′-TGGCTTTCGCTACCTGGAGAGAC, LacZrev 5′-AATCACCGCCGTAAGCCGACCAC, 5loxD 5′-TCCCTTCTGTCCTCCCATCTCC, loxP1 5′-GCTATACGAAGTTATAGCGGCAC, 3loxD 5′-TGGGTGCAAGCCTTTAATCCCC. PCR product sizes with LacZfor/LacZrev primers: *Hormad1*^{insertion} template-208 bp, other alleles-no specific product; with LoxP1/3loxD primers: *Hormad1*^{insertion}, *Hormad1*^{restored} and *Hormad1*^{deletion} templates-267 bp, WT allele-no specific product; with 5loxD/3loxD primers: *Hormad1*^{insertion} and *Hormad1*^{restored} templates-487 bp, WT allele-377 bp, *Hormad1*^{deletion} allele-no specific product. To generate *Hormad1*^{restored}/+ mice, we crossed ES26 derived *Hormad1*^{insertion}/+ mice with hACTB:FLPe transgenic mice[65]. To generate *Hormad1*^{deletion}/+ mice, we crossed *Hormad1*^{restored}/+ with PGK-Cre transgenic mice[66].

Animal experiments

Dmc1, *Spo11* or *Syce2* knockout mice were reported earlier[4, 9, 43]. Experiments were performed in a mixed background (with 75-87.5% contribution from the C57BL/6JOlaHsd inbred line). Whenever possible, experimental animals were compared with litter mate controls or with age-matched non-litter mate controls from the same colony. Although some of the figures show data from juveniles, all of our conclusions were reconfirmed from adult mice (more than 8-weeks-old). In Fig. 2 e-h data points from different ages (16 days and 8 weeks) were pooled when WT and *Hormad1*−/− litter mates were compared, since data at different ages were similar in respect of averages and ranges. HORMAD1 is not detected by western blot in *Hormad1*$^{insertion/insertion}$ testis extract (Supplementary Information, Fig. S2) and HORMAD1 is not detected by immunofluorescence on chromosome axes of *Hormad1*$^{insertion/insertion}$ meiocytes (data not shown), indicating that *Hormad1*^{insertion} is a null allele. All of our conclusions are based on experiments that were performed at least once in the ES26 *Hormad1*^{insertion} lineage. Apart from the kinetic analysis of axis and SC formation all of our conclusions involving experiments with single knockout mice were reconfirmed in the ES21 *Hormad1*^{insertion} and ES26 *Hormad1*^{deletion} lineages. The phenotypes of ES26 *Hormad1*$^{insertion/insertion}$, ES21 *Hormad1*$^{insertion/insertion}$ and ES26

Hormad1$^{deletion/deletion}$ are indistinguishable. Therefore, we do not distinguish between *Hormad1*^{insertion} and *Hormad1*^{deletion} alleles, and we refer to them as the *Hormad1*- allele. ES26 *Hormad1*$^{restored/restored}$ mice are fertile. Testis size and SC formation in spermatocytes are indistinguishable in *Hormad1*$^{restored/restored}$ and WT mice (data not shown), which reconfirms that the phenotypes of *Hormad1*$^{insertion/insertion}$ and *Hormad1*$^{deletion/deletion}$ animals are caused by interference with production of WT *Hormad1* transcripts. For staging embryonic development, the day of detection of a vaginal plug was marked as 0.5 days post coitum (dpc). All animals were used and maintained according to regulations provided by the animal ethics committee of the Technische Universität Dresden.

Immunofluorescence (IF)

Preparation and immunostaining of testis-ovary cryosections and nuclear surface spreads of meiocytes were performed as described previously with a few modifications[40, 67]. Ovaries and testes were fixed for 25 and 40 min, respectively, in 3.6% formaldehyde buffered with pH7.4 100 mM Na-phosphate. 8 μm (ovary) or 7 μm (testis) thick sections were cut from frozen specimens embedded in "O.C.T." (Sakura Finetek Europe). Sections dried onto slides were immunostained following washes in PBS pH7.4 and PBS pH 7.4, 0.1% Triton X-100. IF-TUNEL assay was performed with Millipores′s ApopTag® Plus In Situ Apoptosis Fluorescein Detection Kit (S 7111). Antibodies: as described before[40], rabbit anti-SMC3 (1:200) and rabbit anti-STAG3 (1:500) were gifts from Rolf Jessberger), guinea pig anti-SYCE1 (1:500) and guinea pig anti-SYCE2 (1:200) were gifts from Christer Höög, rabbit anti-RAD51 (1:200, Santa Cruz: sc-8349), rabbit anti-DMC1 (1:50, Santa Cruz: sc-22768), rabbit anti-MSH4 (1:150, Abcam: ab58666), mouse anti-MLH1 (1:50, BD Biosciences: 551092), rabbit anti-ATR (1:300, Calbiochem: PC538), goat anti-BRCA1 (1:30, Santa Cruz: sc-1553), rabbit anti-NOBOX (1:500, Abcam: ab41521), rat IgM anti-GCNA1[68] (1:5, gift from George C. Enders), rabbit anti-cleaved PARP (Asp214) (1:250, Cell Signalling: 9544) and CREST Human centromere auto-antibody HCT-100 (1:50, Cellon SA). For quantification of γH2AX signal in spread spermatocytes (Fig. 4d) matched exposure images were taken as described earlier[40]. We measured total IF signal intensity of γH2AX with ImageJ in squares that covered spread nuclei identified by DAPI staining. Signal intensities were measured in four regions around the examined nuclei to estimate the background. The signal intensity values in Fig. 4d are background corrected. To compare oocyte numbers in adults, we sectioned both ovaries of each mouse (8 μm thick sections), identified oocytes by anti-NOBOX (oocyte marker[69]) immunostaining and counted oocytes in every tenth section. To measure the rate of apoptosis in ovaries of 1 dpp animals, we sectioned both ovaries of each animal (8 μm thick sections). The sections were stained for GCNA1 (oocyte marker[68]) and for cleaved PARP1 (apoptosis marker). The numbers of cleaved PARP-positive and negative oocytes were counted on every eighth section.

Staging meiotic prophase

First, we compared axis development and SC formation in WT nuclear spreads to determine the stages of axis development corresponding to prophase stages. Thereafter, nuclear spreads were staged based on axis development (see details in the legend of Supplementary Information, Fig. S4).

Statistics

Statistical analysis was performed with GraphPad Prism5 and SPSS 11.5 for windows. For the comparison of independent samples, the two-tailed non-parametric Wilcoxon–Mann–Whitney two-sample rank-sum test was used.

Measurement of SPO11-oligonucleotide complexes and testis extracts

Immunoprecipitations of SPO11 and SPO11-oligonucleotide detection were performed as published previously with minor modifications[45]. Both testes from one juvenile or adult mouse were used for each experiment. Testes were decapsulated, then lysed in 800 µl lysis buffer (1% Triton X-100, 400 mM NaCl, 25 mM HEPES-NaOH at pH 7.4, 5 mM EDTA). Lysates were centrifuged at 100,000 rpm (355,040 g) for 25 min in a TLA100.2 rotor. Supernatants were incubated with anti-mSPO11 antibody 180 (5 µg per pair of testes) at 4°C for 1 h, followed by addition of 30-40 µl protein-A–agarose beads (Roche) and incubation for another 3 h. Beads were washed three times with IP buffer (1% Triton X-100, 150 mM NaCl, 15 mM Tris-HCl at pH 8.0). Immunoprecipitates were eluted with Laemmli sample buffer and diluted six- to seven-fold in IP buffer. Eluates were incubated with anti-mSPO11 antibody 180 at 4°C for 1 h, followed by addition of 30-40µl protein-A–agarose beads (Roche) and incubation overnight. Beads were washed three times with IP buffer and twice with buffer NEB4. SPO11-oligonucleotides were radiolabelled at 37 °C for 1 h using terminal deoxynucleotidyl transferase (Fermentas) and [α-32P] dCTP. Beads were washed three times with IP buffer, boiled in Laemmli sample buffer and fractionated on 8% SDS–PAGE. Immunoprecipitates were transferred to a PVDF membrane by semi-dry transfer (Bio-Rad). Radiolabelled species were detected and quantified with Fuji phosphor screens and ImageGuage software. The quantified signal displayed on the figures is background-corrected i.e. the signal found in the *Spo11*−/− testes was subtracted (Fig. 3a, c). To calculate the ratios of testes-weight-normalised SPO11-oligonucleotide levels, the background corrected signal was divided by the weight of the testes. For western analysis, membranes were probed with anti-mSPO11 antibody 180 (1:2000 in PBS containing 0.1% Tween 20 and 5% non-fat dry milk), then horseradish-peroxidase-conjugated protein A (Abcam; 1:10,000 in PBS containing 0.1% Tween 20 and 5% non-fat dry milk), and detected using the ECL+ reagent (GE Healthcare). The anti-SPO11 antibody was produced by the hybridoma cell line 180, which was generated by M.P. Thelen at Lawrence Livermore National Laboratory, California.

For anti-HORMAD1 western blot analysis (Supplementary Information, Fig. S2), total testis extracts were prepared by boiling resuspended testes in Laemmli buffer. Standard methods were used for SDS-PAGE and immunoblotting.

In vitro culture and video microscopy of oocytes

Oocytes were collected from antral follicles of 9-16 weeks old mice into M2 medium (38°C) supplemented with 100 µg/ml dibutyryl cyclic AMP (dbcAMP), which arrested oocytes in germinal vesicle stage (GV). Oocytes were induced to undergo meiotic maturation by rinsing and culture in M2 medium without dbcAMP[70]. Only oocytes where germinal vesicle breakdown (GVBD) was observed within 90 min after release were used for further experiments. Extrusion of the first polar body was determined by visual observation with light microscopy after overnight incubation (approximately 15-19 h after GVBD).

Video microscopy was carried out following injection of GV oocytes with *in vitro*-transcribed mRNAs (Ambion mMessage mMachine kit) coding for histone-H2B-RFP and β-tubulin-GFP[70]. Movies were made on a Nikon TE2000E microscope with PrecisExite High Power LED Fluorescence (LAM 1: 400/465, LAM2: 585), equipped with a temperature chamber (Life Imaging Services), Märzhäuser Scanning Stage, CoolSNAP HQ2 camera, and controlled by Metamorph software. Acquisitions (8z sections, every 2 µm, Plan APO 20x/0.75NA objective) were obtained every 30 min, starting from GVBD+5.5 h. GFP was set to 3% intensity, exposure time to 20 ms, RFP to 5% intensity with a 15 ms exposure time.

Supplementary Material

Refer to Web version on PubMed Central for supplementary material.

Acknowledgments

We thank A. Hientzsch and K. Duerschke for general lab support and technical assistance; R. Jessberger for sharing ideas, antibodies (anti-SYCP3, anti-STAG3 and anti-SMC3) and support; F. Baudat and B. De Massy for providing us with Spo11+/− mice; J. Chen for the anti-TOPBP1 antibody; E. Marcon for the anti-RPA antibody; C. Höög for anti-SYCE1 and anti-SYCE2 antibodies; G.C. Enders for the anti-GCNA antibody; and M.P. Thelen for the anti-SPO11 antibody. We are grateful to M. Siomos and D. Knapp for discussion, revising and proofreading the manuscript. The Deutsche Forschungsgemeinschaft (DFG; grants: TO421/4-1 SPP1384 and TO421/3-1) and the Sächsisches Staatsministerium für Wissenschaft und Kunst supported K.D. and A.T.; Grants HD53855 and HD40916 from the US National Institutes of Health supported J.L., I.R., M.J. and S.K.; ARC (Subvention fixe 1143) and La Ligue Regionale (RS09/75-39) supported K.H. and K.W.; the Medical Research Council UK supported HJC; the DFG research center and cluster of excellence to the Center for Regenerative Therapies Dresden (CRTD) supported the work of K.A.; a CRTD seed grant supported K.A. and A.T.; and an EFRE grant (Europäischer Fonds für Regionale Entwicklung) supported K.A., J.F. and A.F.S.

References

1. Baudat F, de Massy B. Regulating double-stranded DNA break repair towards crossover or non-crossover during mammalian meiosis. Chromosome Res. 2007; 15:565–577. [PubMed: 17674146]
2. Hunter, N. Meiotic recombination in Molecular genetics of recombination. Springer-Verlag; Berlin Heidelberg: 2007.
3. Keeney S, Giroux CN, Kleckner N. Meiosis-specific DNA double-strand breaks are catalyzed by Spo11, a member of a widely conserved protein family. Cell. 1997; 88:375–384. [PubMed: 9039264]
4. Baudat F, Manova K, Yuen JP, Jasin M, Keeney S. Chromosome synapsis defects and sexually dimorphic meiotic progression in mice lacking Spo11. Mol Cell. 2000; 6:989–998. [PubMed: 11106739]
5. Romanienko PJ, Camerini-Otero RD. The mouse *Spo11* gene is required for meiotic chromosome synapsis. Mol Cell. 2000; 6:975–987. [PubMed: 11106738]
6. Sun H, Treco D, Szostak JW. Extensive 3′-overhanging, single-stranded DNA associated with the meiosis-specific double-strand breaks at the ARG4 recombination initiation site. Cell. 1991; 64:1155–1161. [PubMed: 2004421]
7. Hamer G, Novak I, Kouznetsova A, Hoog C. Disruption of pairing and synapsis of chromosomes causes stage-specific apoptosis of male meiotic cells. Theriogenology. 2008; 69:333–339. [PubMed: 17997150]
8. Hamer G, et al. Progression of meiotic recombination requires structural maturation of the central element of the synaptonemal complex. J Cell Sci. 2008; 121:2445–2451. [PubMed: 18611960]
9. Bolcun-Filas E, et al. SYCE2 is required for synaptonemal complex assembly, double strand break repair, and homologous recombination. J Cell Biol. 2007; 176:741–747. [PubMed: 17339376]
10. Bolcun-Filas E, et al. Mutation of the mouse Syce1 gene disrupts synapsis and suggests a link between synaptonemal complex structural components and DNA repair. PLoS Genet. 2009; 5:e1000393. [PubMed: 19247432]
11. de Vries FA, et al. Mouse *Sycp1* functions in synaptonemal complex assembly, meiotic recombination, and XY body formation. Genes Dev. 2005; 19:1376–1389. [PubMed: 15937223]
12. Barchi M, et al. Surveillance of different recombination defects in mouse spermatocytes yields distinct responses despite elimination at an identical developmental stage. Mol Cell Biol. 2005; 25:7203–7215. [PubMed: 16055729]
13. Burgoyne PS, Mahadevaiah SK, Turner JM. The consequences of asynapsis for mammalian meiosis. Nat Rev Genet. 2009; 10:207–216. [PubMed: 19188923]
14. Burgoyne PS, Mahadevaiah SK, Turner JM. The management of DNA double-strand breaks in mitotic G2, and in mammalian meiosis viewed from a mitotic G2 perspective. Bioessays. 2007; 29:974–986. [PubMed: 17876782]

15. Aravind L, Koonin EV. The HORMA domain: a common structural denominator in mitotic checkpoints, chromosome synapsis and DNA repair. Trends Biochem Sci. 1998; 23:284–286. [PubMed: 9757827]
16. Martinez-Perez E, Villeneuve AM. HTP-1-dependent constraints coordinate homolog pairing and synapsis and promote chiasma formation during *C. elegans* meiosis. Genes Dev. 2005; 19:2727–2743. [PubMed: 16291646]
17. Nonomura K, Nakano M, Eiguchi M, Suzuki T, Kurata N. PAIR2 is essential for homologous chromosome synapsis in rice meiosis I. J Cell Sci. 2006; 119:217–225. [PubMed: 16410547]
18. Couteau F, Zetka M. HTP-1 coordinates synaptonemal complex assembly with homolog alignment during meiosis in *C. elegans*. Genes Dev. 2005; 19:2744–2756. [PubMed: 16291647]
19. Goodyer W, et al. HTP-3 links DSB formation with homolog pairing and crossing over during *C. elegans* meiosis. Dev Cell. 2008; 14:263–274. [PubMed: 18267094]
20. Martinez-Perez E, et al. Crossovers trigger a remodeling of meiotic chromosome axis composition that is linked to two-step loss of sister chromatid cohesion. Genes Dev. 2008; 22:2886–2901. [PubMed: 18923085]
21. Severson AF, Ling L, van Zuylen V, Meyer BJ. The axial element protein HTP-3 promotes cohesin loading and meiotic axis assembly in C. elegans to implement the meiotic program of chromosome segregation. Genes Dev. 2009; 23:1763–1778. [PubMed: 19574299]
22. Zetka MC, Kawasaki I, Strome S, Muller F. Synapsis and chiasma formation in *Caenorhabditis elegans* require HIM-3, a meiotic chromosome core component that functions in chromosome segregation. Genes Dev. 1999; 13:2258–2270. [PubMed: 10485848]
23. Couteau F, Nabeshima K, Villeneuve A, Zetka M. A component of *C. elegans* meiotic chromosome axes at the interface of homolog alignment, synapsis, nuclear reorganization, and recombination. Curr Biol. 2004; 14:585–592. [PubMed: 15062099]
24. MacQueen AJ, Colaiacovo MP, McDonald K, Villeneuve AM. Synapsis-dependent and -independent mechanisms stabilize homolog pairing during meiotic prophase in C. elegans. Genes Dev. 2002; 16:2428–2442. [PubMed: 12231631]
25. Nabeshima K, Villeneuve AM, Hillers KJ. Chromosome-wide regulation of meiotic crossover formation in Caenorhabditis elegans requires properly assembled chromosome axes. Genetics. 2004; 168:1275–1292. [PubMed: 15579685]
26. Sanchez-Moran E, Santos JL, Jones GH, Franklin FC. ASY1 mediates AtDMC1-dependent interhomolog recombination during meiosis in Arabidopsis. Genes Dev. 2007; 21:2220–2233. [PubMed: 17785529]
27. Hollingsworth NM, Byers B. *HOP1*: a yeast meiotic pairing gene. Genetics. 1989; 121:445–462. [PubMed: 2653960]
28. Loidl J, Klein F, Scherthan H. Homologous pairing is reduced but not abolished in asynaptic mutants of yeast. J Cell Biol. 1994; 125:1191–1200. [PubMed: 8207053]
29. Schwacha A, Kleckner N. Identification of joint molecules that form frequently between homologs but rarely between sister chromatids during yeast meiosis. Cell. 1994; 76:51–63. [PubMed: 8287479]
30. Hollingsworth NM, Ponte L. Genetic interactions between HOP1, RED1 and MEK1 suggest that MEK1 regulates assembly of axial element components during meiosis in the yeast Saccharomyces cerevisiae. Genetics. 1997; 147:33–42. [PubMed: 9286666]
31. Bailis JM, Smith AV, Roeder GS. Bypass of a meiotic checkpoint by overproduction of meiotic chromosomal proteins. Mol Cell Biol. 2000; 20:4838–4848. [PubMed: 10848609]
32. Woltering D, et al. Meiotic segregation, synapsis, and recombination checkpoint functions require physical interaction between the chromosomal proteins Red1p and Hop1p. Mol Cell Biol. 2000; 20:6646–6658. [PubMed: 10958662]
33. Niu H, et al. Partner choice during meiosis is regulated by Hop1-promoted dimerization of Mek1. Mol Biol Cell. 2005; 16:5804–5818. [PubMed: 16221890]
34. Niu H, et al. Mek1 kinase is regulated to suppress double-strand break repair between sister chromatids during budding yeast meiosis. Mol Cell Biol. 2007; 27:5456–5467. [PubMed: 17526735]

35. Carballo JA, Johnson AL, Sedgwick SG, Cha RS. Phosphorylation of the axial element protein Hop1 by Mec1/Tel1 ensures meiotic interhomolog recombination. Cell. 2008; 132:758–770. [PubMed: 18329363]
36. Joshi N, Barot A, Jamison C, Borner GV. Pch2 links chromosome axis remodeling at future crossover sites and crossover distribution during yeast meiosis. PLoS Genet. 2009; 5:e1000557. [PubMed: 19629172]
37. Zetka M. Homologue pairing, recombination and segregation in Caenorhabditis elegans. Genome Dyn. 2009; 5:43–55. [PubMed: 18948706]
38. Hayashi M, Chin GM, Villeneuve AM. C. elegans germ cells switch between distinct modes of double-strand break repair during meiotic prophase progression. PLoS Genet. 2007; 3:e191. [PubMed: 17983271]
39. Fukuda T, Daniel K, Wojtasz L, Toth A, Hoog C. A novel mammalian HORMA domain-containing protein, HORMAD1, preferentially associates with unsynapsed meiotic chromosomes. Exp Cell Res. 2010; 316:158–171. [PubMed: 19686734]
40. Wojtasz L, et al. Mouse HORMAD1 and HORMAD2, two conserved meiotic chromosomal proteins, are depleted from synapsed chromosome axes with the help of TRIP13 AAA-ATPase. PLoS Genet. 2009; 5:e1000702. [PubMed: 19851446]
41. Shin YH, et al. Hormad1 mutation disrupts synaptonemal complex formation, recombination, and chromosome segregation in mammalian meiosis. PLoS Genet. 2010; 6:e1001190. [PubMed: 21079677]
42. Ahmed EA, de Rooij DG. Staging of mouse seminiferous tubule cross-sections. Methods Mol Biol. 2009; 558:263–277. [PubMed: 19685330]
43. Pittman DL, et al. Meiotic prophase arrest with failure of chromosome synapsis in mice deficient for *Dmc1*, a germline-specific RecA homolog. Mol Cell. 1998; 1:697–705. [PubMed: 9660953]
44. Yoshida K, et al. The mouse *RecA*-like gene *Dmc1* is required for homologous chromosome synapsis during meiosis. Mol Cell. 1998; 1:707–718. [PubMed: 9660954]
45. Neale MJ, Pan J, Keeney S. Endonucleolytic processing of covalent protein-linked DNA double-strand breaks. Nature. 2005; 436:1053–1057. [PubMed: 16107854]
46. Moens PB, Marcon E, Shore JS, Kochakpour N, Spyropoulos B. Initiation and resolution of interhomolog connections: crossover and non-crossover sites along mouse synaptonemal complexes. J Cell Sci. 2007; 120:1017–1027. [PubMed: 17344431]
47. Baker SM, et al. Involvement of mouse Mlh1 in DNA mismatch repair and meiotic crossing over. Nat Genet. 1996; 13:336–342. [PubMed: 8673133]
48. Marcon E, Moens P. MLH1p and MLH3p localize to precociously induced chiasmata of okadaic-acid-treated mouse spermatocytes. Genetics. 2003; 165:2283–2287. [PubMed: 14704203]
49. Fernandez-Capetillo O, Liebe B, Scherthan H, Nussenzweig A. H2AX regulates meiotic telomere clustering. J Cell Biol. 2003; 163:15–20. [PubMed: 14530383]
50. Bellani MA, Romanienko PJ, Cairatti DA, Camerini-Otero RD. SPO11 is required for sex-body formation, and *Spo11* heterozygosity rescues the prophase arrest of *Atm*−/− spermatocytes. J Cell Sci. 2005; 118:3233–3245. [PubMed: 15998665]
51. Moens PB, et al. The association of ATR protein with mouse meiotic chromosome cores. Chromosoma. 1999; 108:95–102. [PubMed: 10382071]
52. Plug AW, et al. Changes in protein composition of meiotic nodules during mammalian meiosis. J Cell Sci. 1998; 111(Pt 4):413–423. [PubMed: 9443891]
53. Plug AW, et al. ATM and RPA in meiotic chromosome synapsis and recombination. Nat Genet. 1997; 17:457–461. [PubMed: 9398850]
54. Keegan KS, et al. The Atr and Atm protein kinases associate with different sites along meiotically pairing chromosomes. Genes Dev. 1996; 10:2423–2437. [PubMed: 8843195]
55. Perera D, et al. TopBP1 and ATR colocalization at meiotic chromosomes: role of TopBP1/Cut5 in the meiotic recombination checkpoint. Mol Biol Cell. 2004; 15:1568–1579. [PubMed: 14718568]
56. Turner JM, et al. BRCA1, histone H2AX phosphorylation, and male meiotic sex chromosome inactivation. Curr Biol. 2004; 14:2135–2142. [PubMed: 15589157]

57. Turner JM, et al. Silencing of unsynapsed meiotic chromosomes in the mouse. Nat Genet. 2005; 37:41–47. [PubMed: 15580272]
58. Baarends WM, et al. Silencing of unpaired chromatin and histone H2A ubiquitination in mammalian meiosis. Mol Cell Biol. 2005; 25:1041–1053. [PubMed: 15657431]
59. Turner JM, Mahadevaiah SK, Ellis PJ, Mitchell MJ, Burgoyne PS. Pachytene asynapsis drives meiotic sex chromosome inactivation and leads to substantial postmeiotic repression in spermatids. Dev Cell. 2006; 10:521–529. [PubMed: 16580996]
60. Mahadevaiah SK, et al. Extensive meiotic asynapsis in mice antagonises meiotic silencing of unsynapsed chromatin and consequently disrupts meiotic sex chromosome inactivation. J Cell Biol. 2008; 182:263–276. [PubMed: 18663141]
61. Royo H, et al. Evidence that meiotic sex chromosome inactivation is essential for male fertility. Curr Biol. 2010; 20:2117–2123. [PubMed: 21093264]
62. Martini E, Diaz RL, Hunter N, Keeney S. Crossover homeostasis in yeast meiosis. Cell. 2006; 126:285–295. [PubMed: 16873061]
63. Testa G, et al. A reliable lacZ expression reporter cassette for multipurpose, knockout-first alleles. Genesis. 2004; 38:151–158. [PubMed: 15048813]
64. Zhang Y, Buchholz F, Muyrers JP, Stewart AF. A new logic for DNA engineering using recombination in Escherichia coli. Nat Genet. 1998; 20:123–128. [PubMed: 9771703]
65. Rodriguez CI, et al. High-efficiency deleter mice show that FLPe is an alternative to Cre-loxP. Nat Genet. 2000; 25:139–140. [PubMed: 10835623]
66. Lallemand Y, Luria V, Haffner-Krausz R, Lonai P. Maternally expressed PGK-Cre transgene as a tool for early and uniform activation of the Cre site-specific recombinase. Transgenic Res. 1998; 7:105–112. [PubMed: 9608738]
67. Hodges CA, Hunt PA. Simultaneous analysis of chromosomes and chromosome-associated proteins in mammalian oocytes and embryos. Chromosoma. 2002; 111:165–169. [PubMed: 12355205]
68. Enders GC, May JJ 2nd. Developmentally regulated expression of a mouse germ cell nuclear antigen examined from embryonic day 11 to adult in male and female mice. Dev Biol. 1994; 163:331–340. [PubMed: 8200475]
69. Suzumori N, Yan C, Matzuk MM, Rajkovic A. Nobox is a homeobox-encoding gene preferentially expressed in primordial and growing oocytes. Mech Dev. 2002; 111:137–141. [PubMed: 11804785]
70. Niault T, et al. Changing Mad2 levels affects chromosome segregation and spindle assembly checkpoint control in female mouse meiosis I. PLoS One. 2007; 2:e1165. [PubMed: 18043727]

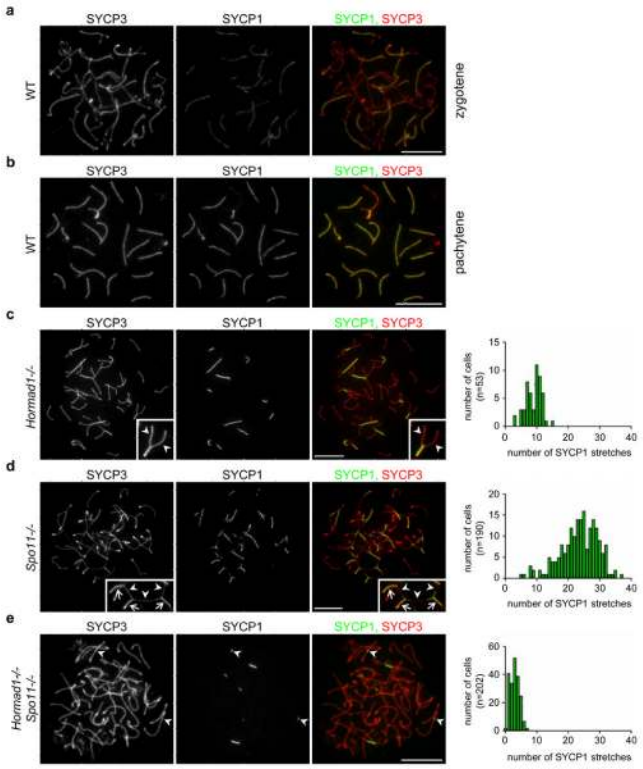

Figure 1. HORMAD1 promotes SC formation independently of DSB-dependent processes

Images of SYCP3 (chromosome axis) and SYCP1 (SC transverse filament), detected by immunofluorescence (IF) on nuclear spreads of WT zygotene (**a**), WT pachytene (**b**) and mutant zygotene-pachytene spermatocytes (**c-e** left) collected from 14-weeks-old mice. The frequency distribution of SC stretches in mutant zygotene-pachytene spermatocytes is shown (**c-e** right). **c**, SC formation is never completed on all autosomes in *Hormad1−/−* cells, and unlike in SC transverse filament mutant meiocytes, where unsynapsed chromosomes align along their length[8-11], unsynapsed chromosomes do not align in *Hormad1−/−* spermatocytes. Nevertheless, robust stretches of SC frequently form between chromosomes that appear homologous based on their similar axis length. See enlarged view of boxed partially synapsed autosome: unsynapsed axes (arrowheads) are of similar lengths. **d**, In contrast, SCs connect multiple non-homologous axes, thereby creating a meshwork of interconnected axes in *Spo11−/−* mutant, in which strand invasion and homology search is not possible due to lack of DSBs. See enlarged view of boxed chromosome axes: arrowheads mark unsynapsed, arrows mark synapsed axes. **e**. Both the number and the length of SYCP1 stretches are reduced in *Hormad1−/− Spo11−/−* spermatocytes relative to the single mutants. The majority (61% in n=144 cells) of the remaining SYCP1 stretches is unambiguously linked to a single chromosome axis (arrowheads) indicating that SYCP1 stretches do not necessarily mark inter-chromosomal SCs. Bars, 10 μm.

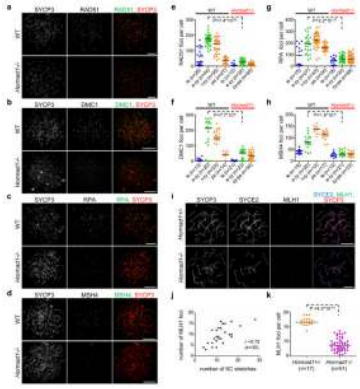

Figure 2. Numbers of early, intermediate and late recombination protein foci are reduced in the absence of HORMAD1 in prophase meiocytes

a-d, SYCP3 and either RAD51 (**a**) DMC1 (**b**), RPA (**c**) or MSH4 (**d**) are detected on nuclear spreads of typical early-mid-zygotene WT and *Hormad1*−/− spermatocytes from 16-days-old mice. Bars, 10 μm. **e-h**, Foci numbers of early (RAD51-**e**, DMC1-**f**) and intermediate (RPA-**g**, MSH4-**h**) recombination proteins during leptotene (le) and early-mid-zygotene (e-zy) in WT and *Hormad1*−/−; late-zygotene (l-zy) and pachytene (pa) in WT and zygotene-pachytene (zy-pa) in *Hormad1*−/− spermatocytes. Median foci numbers are marked. During the comparable early-mid-zygotene stage, a three- to six-fold reduction (highly significant by Mann–Whitney test) is observed in recombination protein foci numbers in the mutant relative to WT. **i-k**, Focus numbers of the CO marker MLH1 are reduced in the absence of HORMAD1 in oocytes. **i**, SYCP3 (chromosome axis), SYCE2 (SC central element) and MLH1 were detected by IF in nuclear spreads of *Hormad1*+/− and *Hormad1*−/− oocytes from 19.5 dpc foetuses (a stage when most oocytes are in the late-pachytene or diplotene stage in WT). Fewer chromosome axis-associated MLH1 foci are detected in *Hormad1*−/− oocytes than in *Hormad1*+/− oocytes. Note that the majority of MLH1 foci (78%, n=51 cells) are observed on synapsed axes in the mutant. Bars, 10 μm. **j**, Scatter plot shows positive correlation (Spearman's r=0.72, n=30) between MLH1 foci numbers and the number of SC stretches (immunostaining for SYCE1 or SYCE2) in *Hormad1*−/− oocytes, indicating that DSBs might be repaired as COs preferentially in chromosome regions that align and synapse, or that synapsis occurs preferentially where COs are successfully designated. **k**, Chromosome axis-associated MLH1 focus numbers are reduced approximately three-fold in *Hormad1*−/− oocytes from 18.5-19.5 dpc foetuses relative to *Hormad1*+/− oocytes. Median focus numbers are marked by horizontal lines.

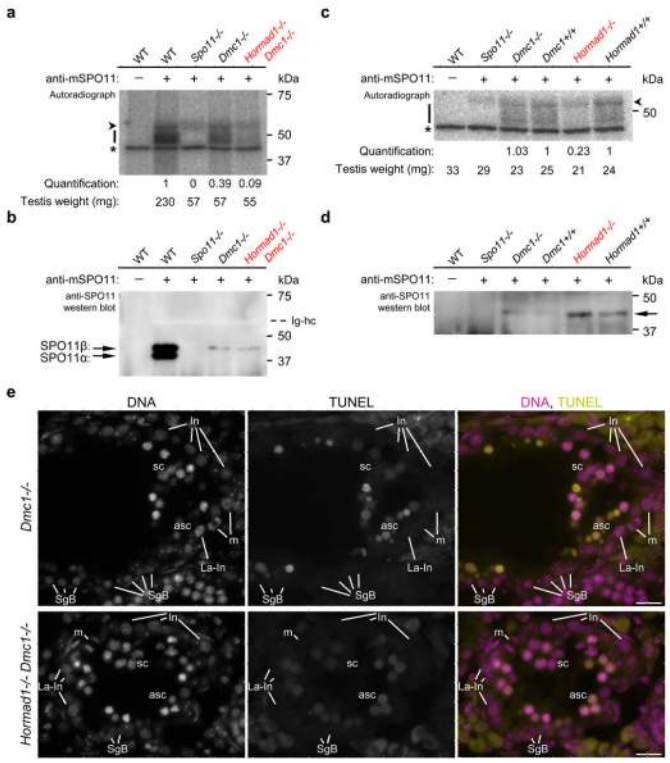

Figure 3. Amounts of SPO11-oligonucleotide complexes in testes are reduced in the absence of HORMAD1

a, c, Measurement of SPO11-oligonucleotide complexes in testes of adult 14-weeks-old (**a**) and juvenile 14 dpp (**c**) mice. SPO11-oligonucleotide complexes were immunoprecipitated with or without anti-SPO11 antibodies, and covalently-linked oligonucleotides were radioactively labelled. Each sample represents one testis-equivalent SPO11-oligonucleotide complexes. Bars mark SPO11-specific signals and asterisks indicate non-specific labelling of a contaminant in the terminal deoxytransferase preparations. Arrowhead marks an artifactual radioactive signal attributable to presence of immunoglobulin heavy chain (Ig-hc in **b**). Quantified radioactive signals in the mutants have been background-corrected and normalised: in **a** signals are normalised to the adult WT control; in **c** *Dmc1−/−* and *Hormad1−/−* signals are normalised to their litter mate *Dmc1*+/+ and *Hormad1*+/+ controls, respectively (see Methods). Blots of immunoprecipitates from **a** and **c** were probed with anti-SPO11 antibodies in **b** and **d,** respectively. **b**, In WT adults, two alternative forms of SPO11 (α and β) are present[5]. Total SPO11 amounts are similar in *Dmc1−/−* and *Hormad1−/− Dmc1−/−* mutants, and are lower in the mutants than in WT. Only SPO11β, the form that appears early in meiosis, is detected in the mutants. Arrowhead marks the immunoglobulin heavy chain (bleached out signal). Mid-pachytene spermatogenic block in the mutants (**e**) is the likely cause of reduced SPO11 amounts in *Dmc1−/−* and *Hormad1−/− Dmc1−/−* testes, and of reduced SPO11-oligonucleotide amounts in *Dmc1−/−* testes[12, 43, 44]. **d**, In juveniles, total SPO11 protein levels are low and only the long β form of SPO11 (arrow) is detectable[5]. For full scan gel-images of **a-d** see Supplementary Information, Fig, S10. **e**, DNA was detected by DAPI, and apoptosis was detected by IF-TUNEL assay on cryosections of testes of 15-weeks-old mice. *Dmc1−/−* and *Hormad1−/− Dmc1−/−* spermatocytes undergo apoptosis in stage IV tubules as identified by the concomitant presence of intermediate spermatogonia (In), late-prometaphase intermediate spermatogonia (La-In), mitotic intermediate spermatogonia (m) and spermatogonia B (SgB). Both non-apoptotic (sc) and apoptotic (asc) spermatocytes are present in the stage IV tubules shown.

Spermatocytes are fully eliminated upon progression to stage V (data not shown). Bars, 20 μm.

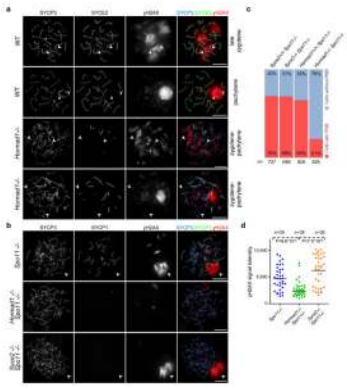

Figure 4. HORMAD1 is required for sex body and pseudo-sex body formation in the *Spo11*+/+ and *Spo11*−/− backgrounds, respectively

a, SYCP3 (chromosome axis), SYCE2 (SC central element) and γH2AX were detected in nuclear spreads of WT late-zygotene and pachytene, and *Hormad1*−/− zygotene-pachytene spermatocytes collected from 16-days-old mice. Matched exposure images of γH2AX are shown. In WT late-zygotene spermatocytes, γH2AX chromatin domains associate with unsynapsed chromosome axes. In WT pachytene cells, unsynapsed regions of X and Y sex chromosome axes (marked by x and y) are surrounded by one large γH2AX-rich chromatin domain, the sex body. Anti-γH2AX staining is patchy in the majority (59%) of *Hormad1*−/− spermatocytes, with no clear correlation between lack of synapsis and γH2AX localisation (third row). A few large γH2AX-rich chromatin domains form in a minority of *Hormad1*−/− spermatocytes (41%, n=512), but only a subset of unsynapsed axes overlap with γH2AX-rich chromatin, and synapsed axes overlapping with γH2AX-rich chromatin domains are also observed regularly (bottom row). Arrowheads mark two unsynapsed axes in WT late-zygotene and in each mutant cell. Bars, 10 μm. **b**, Matched exposure images of SYCP3 (chromosome axis), SYCP1 (SC transverse filament) and γH2AX in nuclear spreads of *Spo11*−/− , *Hormad1*−/− *Spo11*−/− and *Syce2*−/− *Spo11*−/− spermatocytes of adult (9-weeks-old) mice. Large γH2AX-rich chromatin domains-pseudo-sex bodies (marked by arrowheads) frequently form in *Spo11*−/− and *Syce2*−/− *Spo11*−/− spermatocytes. Bars, 10 μm. **c**, Quantification of pseudo-sex body formation in spermatocytes with full-length chromosome axes (collected from 24-days-old mice). The percentage of cells with no pseudo-sex body (cells without PSB) or with one to three clear pseudo-sex bodies (cells with PSB) is shown. **d**, Quantification of γH2AX signal in spermatocytes with full-length chromosome axes (collected from 24-days-old mice) shows a significant reduction in total nuclear γH2AX amounts in *Hormad1*−/− *Spo11*−/− relative to *Spo11*−/− and *Syce2*−/− *Spo11*−/− (Mann–Whitney test).

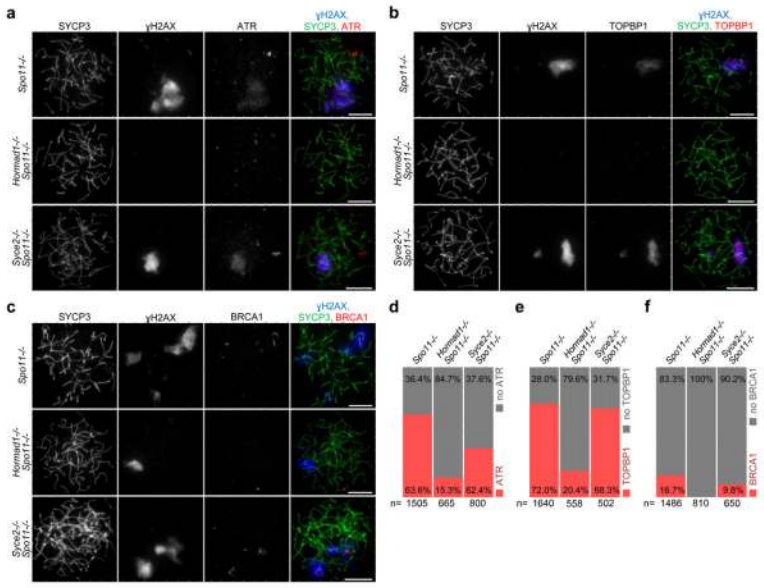

Figure 5. I HORMAD1 is required for efficient accumulation of ATR, TOPBP1 and BRCA1 on chromatin in the absence of programmed DSBs

Matched exposure images of SYCP3 (chromosome axis), γH2AX and either ATR (**a**), TOPBP1 (**b**) or BRCA1 (**c**) in nuclear spreads of spermatocytes collected from 24-days-old mice. *Spo11−/−* and *Syce2−/− Spo11−/−* spermatocytes are shown with cloud-like ATR (**a**) or TOPBP1 (**b**) accumulation or with BRCA1 localised to axes (**c**) in γH2AX-marked pseudo-sex bodies. In **a** and **b,** *Hormad1−/− Spo11−/−* cells are shown without a pseudo-sex body and without ATR or TOPBP1 accumulation on chromatin, respectively. In **c**, *Hormad1−/− Spo11−/−* cell is shown with a pseudo-sex body, within which no BRCA1 association with the axis was detected. Note that only a small minority of *Hormad1−/− Spo11−/−* spermatocytes shows pseudo-sex body-like accumulation of γH2AX (Fig. 4c). Bars, 10 μm. **d-f,** Frequency of cloud-like ATR (**d**) and TOPBP1 (**e**) accumulation and frequency of BRCA1 association with axes (**f**) in spermatocytes with fully formed chromosome axes. ATR- and TOPBP1-rich chromatin domains are frequently observed in *Spo11−/−* and *Syce2−/− Spo11−/−* spermatocytes, and BRCA1 association with axes is also observed in these mutants. ATR and TOPBP1 are virtually absent from chromatin in the large majority of *Hormad1−/− Spo11−/−* cells, and BRCA1 localisation to axes was never observed in *Hormad1−/− Spo11−/−* spermatocytes.

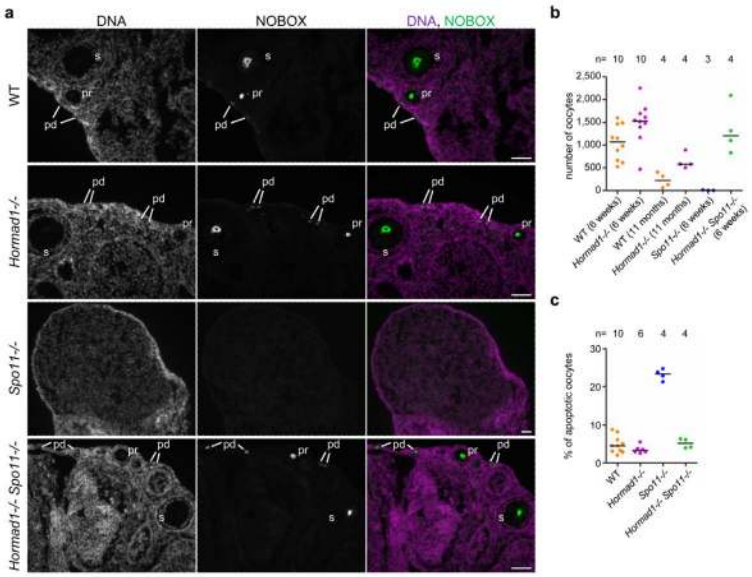

Figure 6. I Lack of HORMAD1 allows survival of oocytes in the SC-defective *Spo11−/−* mutant

a, NOBOX (postnatal oocyte marker) was detected by IF on cryosections of ovaries from 6-weeks-old mice. DNA was detected by DAPI. Oocytes in primordial (pd), primary (pr) and secondary (s) follicular stages are shown in WT, *Hormad1−/−* and *Hormad1−/− Spo11−/−* ovaries. In the SC-defective *Spo11−/−* mutant, oocyte numbers are strongly reduced. A lower magnification section of a *Spo11−/−* ovary is shown to better illustrate the absence of oocytes. Bars, 50 μm. **b**, Sum of oocyte numbers on every tenth section of sectioned-through ovary pairs at the indicated ages. Each data point represents a mouse. **c**, Fraction of apoptotic oocytes in the ovaries of 1-day-old (1 dpp) mice of indicated genotypes. Horizontal lines show medians in **b** and **c**.

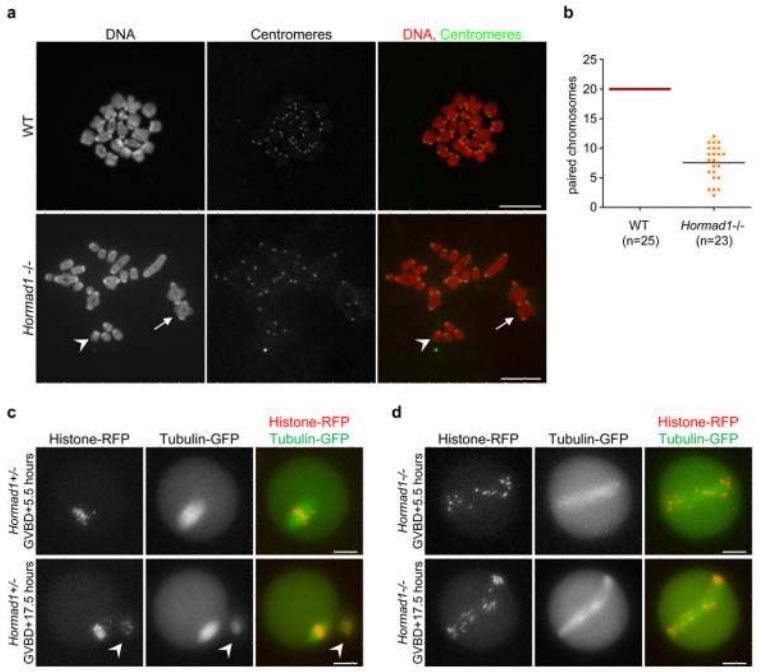

Figure 7. Reduced numbers of chiasmata form in *Hormad1 −/−* oocytes

a, Centromeres were detected by IF and DNA was detected by propidium iodide on nuclear spreads of *in vitro*-matured metaphase stage oocytes. In WT cells, 20 pairs of chromosomes are connected by chiasmata. In the *Hormad1 −/−* mutant, a large fraction of chromosomes does not have chiasmata (one such chromosome is marked by arrowhead). Arrow marks a pair of chromosomes connected via a chiasma in the mutant oocyte. Note that bivalents are symmetrical and chiasmata form between chromosomes of identical length in the mutant, indicating that CO formation took place between homologous chromosomes. Chromosomes scatter over a larger area during nuclear spreading in the mutant, therefore it was not possible to include all 40 chromosomes of a meiosis I oocyte in the image. Bars, 10 μm. **b**, The average numbers of paired chromosomes connected by chiasmata (marked by line) are reduced nearly three-fold in *in vitro*-matured *Hormad1 −/−* oocytes relative to WT oocytes. **c** and **d,** mRNAs encoding β-tubulin-GFP and histone H2B-RFP were injected into WT (**c**) and *Hormad1 −/−* (**d**) oocytes during the germinal vesicle stage (prophase), and the oocytes were matured *in vitro*. The fluorescent proteins in the oocytes were imaged 5.5 hours after germinal vesicle break down (GVBD), at a time when WT oocytes are in the first meiotic metaphase, and 17.5 hours after GVBD, at a time when WT oocytes are arrested in the second meiotic metaphase. A polar body (marked by arrowhead in **c**), which was extruded 7 hours after GVBD (Supplementary Information, Movie 1) is observed next to the metaphase II stage WT oocyte at the 17.5 hour time point. In the *Hormad1 −/−* oocyte (**d**), the meiotic spindle is abnormally long and chromosomes fail to align at both time points. Meiotic anaphase did not take place in the displayed *Hormad1 −/−* oocyte (Supplementary Information, Movie 2), and no polar body can be observed at either time points (**d**). Bars, 20 μm.

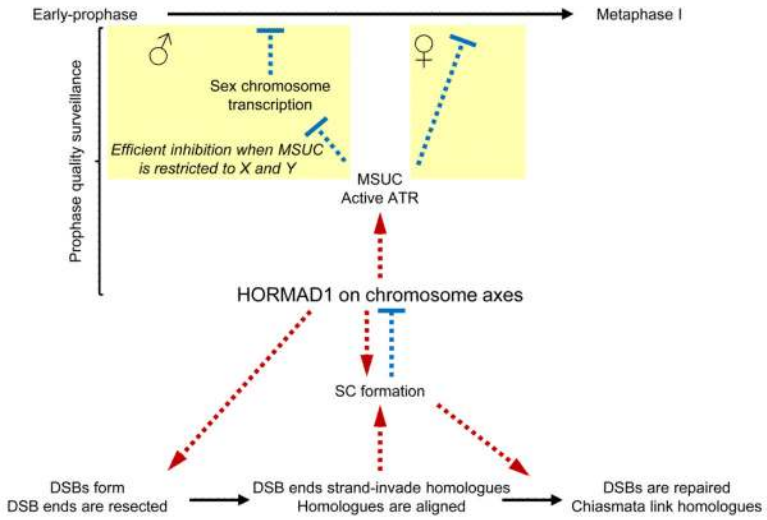

Figure 8. Model for meiotic progression: negative feedback-loop of HORMAD1 and SC coordinates homology search and meiotic progression

Processes, activation-promotion and inhibition are marked by continuous black arrows, red dashed arrows and blue flat-ended dashed arrows, respectively. HORMAD1 associates with forming chromosome axes at the beginning of meiosis where it promotes DSB formation and/or processing of DSBs. It thereby ensures that adequate numbers of single-stranded DSBs are available for homology search. As part of the homology search process DSB ends strand-invade into homologues. Multiple strand invasion events along the length of chromosomes lead to full alignment of pairs of homologues, which is a prerequisite for the completion of SC formation. HORMAD1 also promotes SC formation through a mechanism that is independent of homology search. SC formation leads to depletion of HORMAD1 from axes and down-regulation of HORMAD1 function[40]. Hence, in spermatocytes, full autosomal SC formation leads to a restriction of HORMAD1 and ATR activity to sex chromosomes, thereby promoting efficient silencing of sex chromosomes, which is a prerequisite for progression beyond mid-pachytene[13, 60, 61]. In oocytes, completion of SC formation on all chromosomes leads to complete inactivation of HORMAD1, which in turn leads to down-regulation of ATR and MSUC. Since sustained ATR activity and/or sustained MSUC is believed to block progression beyond meiotic prophase[13], full SC formation and HORMAD1 inactivation link successful homologue alignment with progression beyond meiotic prophase. Note that successful DSB repair is probably also required for full down-regulation of ATR activity and for meiotic progression in oocytes (for the sake of simplicity, this branch of the prophase checkpoint is not displayed in the model).